Acta Biomaterialia 200 (2025) 641–652

Contents lists available at ScienceDirect

Acta Biomaterialia

journal homepage: www.elsevier.com/locate/actbio

Full length article

Vincristine/Volasertib polymersome injection enables high-efficiency synergistic treatment of acute lymphoblastic leukemia

Qing Deng [a,1], Shujing Yue [a,1], Fengtao You [b], Zhenzhen Zhai [a], Huanli Sun [a,*], Lanlan Liang [a], Chenming Li [a], Lin Yang [b,c,*], Zhiyuan Zhong [a,d,e,*]

[a] State Key Laboratory of Bioinspired Interfacial Materials Science, and Biomedical Polymers Laboratory, Chemical Engineering and Materials Science, College of Chemistry, Soochow University, Suzhou 215123, China
[b] PersonGen BioTherapeutics (Suzhou) Co., Ltd., Suzhou, China
[c] Cyrus Tang Medical Institute, Collaborative Innovation Center of Hematology, Soochow University, Suzhou 215123, China
[d] College of Pharmaceutical Sciences, Soochow University, Suzhou 215123, China
[e] International College of Pharmaceutical Innovation, Soochow University, Suzhou 215222, China

ARTICLE INFO

Keywords:
Polymersomes
Drug delivery
Combination therapy
Leukemia
Nanomedicines

ABSTRACT

Acute lymphoblastic leukemia (ALL), one of the most frequently diagnosed malignancies in children, is associated with a high relapse rate and drug resistance, even with intensive multidrug chemotherapy regimens. The rational combination with molecular targeted agents holds promise for sensitizing patients to chemotherapies and overcoming drug resistance. However, precise codelivery of different drugs *in vivo* is challenging, often leading to suboptimal therapeutic effects. Herein, we report a vincristine/volasertib polymersome (Ps-VCR/Vol)-based nanocombo for synergistic inhibition of microtubules and polo-like kinase 1, enabling high-efficacy treatment of ALL *in vivo*. Ps-VCR/Vol, which has a small size (~26 nm) and tailored VCR/Vol mass ratios from 1:12 to 1:48, exhibited strong synergy in different ALL cells, with 3.3–6.8-fold greater anti-ALL activity than the free VCR/Vol combination. Intriguingly, treatment with Ps-VCR/Vol at a VCR/Vol dosage of 0.25/6 mg/kg markedly inhibited leukemia progression and invasion in orthotopic CCRF-CEM, Nalm-6-Luc and patient-derived xenograft ALL mouse models without inducing toxicity, resulting in a significantly prolonged survival time compared with that of the free drug combination and single-drug polymersome formulations. Ps-VCR/Vol polymersome injection provides a powerful synergistic combination therapy for ALL.

Statement of significance: Multidrug combination therapies have increased the remission rates of acute lymphoblastic leukemia (ALL) patients. However, the therapeutic efficacy remains suboptimal due to the dissimilar physicochemical properties of the different drugs involved, and overlapping toxicities pose a critical concern. Herein, we show that intelligent polymersomes mediate the precise codelivery of vincristine sulfate (VCR), a frontline drug for ALL, and volasertib (Vol), a polo-like kinase 1 inhibitor, enabling synergistic treatment of ALL. Compared with free VCR/Vol, VCR/Vol polymersomes with tailored drug ratios substantially inhibited leukemia progression in both cell line- and patient-derived orthotopic ALL models without inducing toxicity, leading to a significant survival benefit. This synergistic polymersome injection may provide a powerful and safe combination therapy for ALL patients.

1. Introduction

Acute lymphoblastic leukemia (ALL) is one of the most common malignancies in pediatric patients and is characterized by the abnormal proliferation of lymphoid progenitor cells within the bone marrow and blood as well as their extramedullary invasion [1–4]. Over the past decades, the optimization of multidrug combination-based intensive chemotherapy has markedly improved the remission and cure rates of ALL patients [5–7]. However, a significant number of patients experience drug resistance and relapse, leading to a poor prognosis, with a 5-year survival rate of only approximately 40 % [8]. Furthermore, survivors often endure heavily compromised quality of life as a result of

* Corresponding authors.
E-mail addresses: sunhuanli@suda.edu.cn (H. Sun), yanglin@suda.edu.cn (L. Yang), zyzhong@suda.edu.cn (Z. Zhong).
[1] These authors contributed equally to the work.

https://doi.org/10.1016/j.actbio.2025.05.041
Received 31 December 2024; Received in revised form 12 May 2025; Accepted 15 May 2025
Available online 16 May 2025

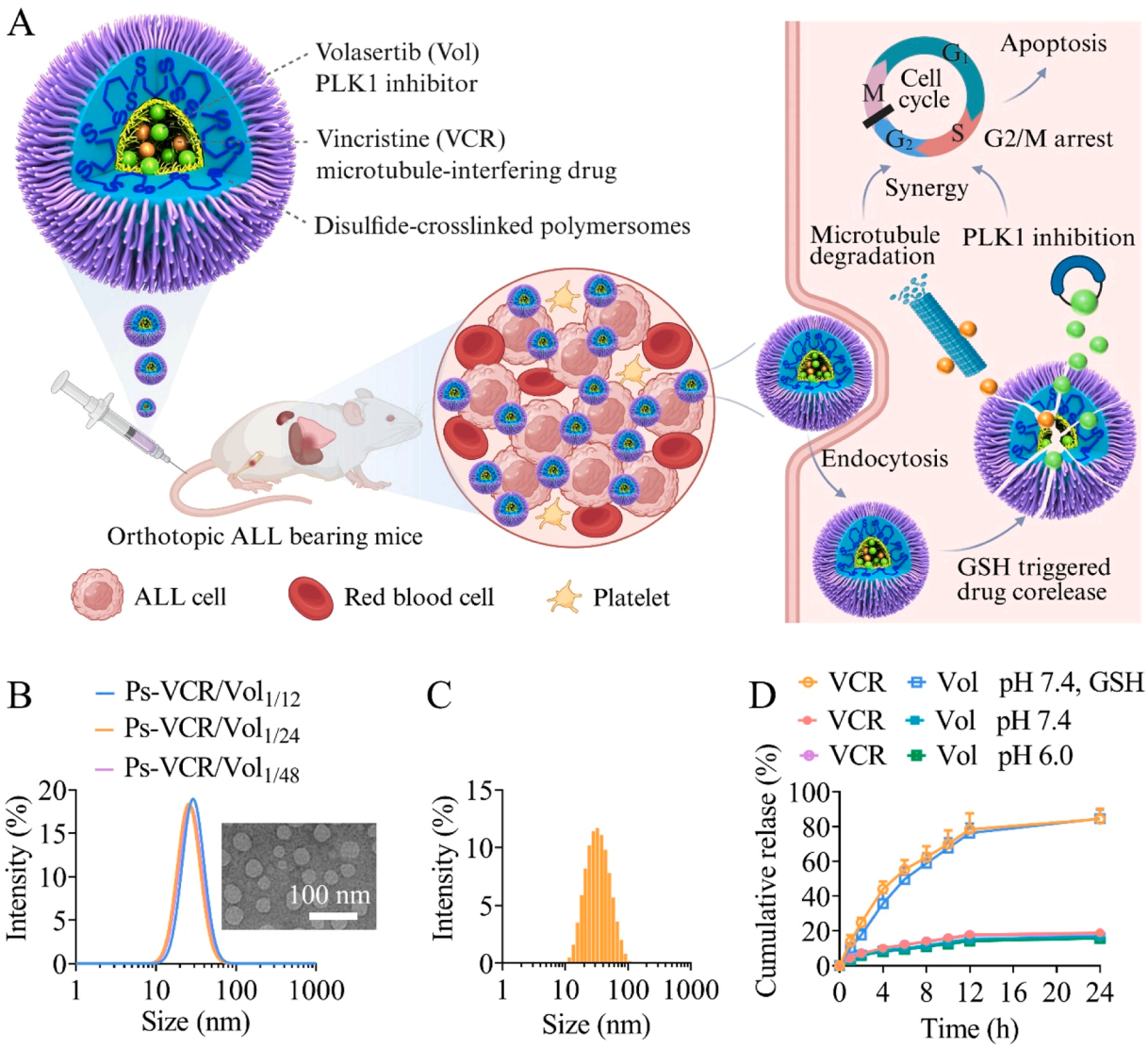

Fig. 1. Vincristine/volasertib polymersome injection (Ps-VCR/Vol) for synergistic therapy of ALL and characterization of Ps-VCR/Vol. (A) Schematic showing synergistic Ps-VCR/Vol for high-efficiency combination therapy of ALL. (B) Size distributions of Ps-VCR/Vol with different VCR/Vol mass ratios. Inset: transmission electron microscopy (TEM) image of Ps-VCR/$Vol_{1/24}$. (C) Size distribution of Ps-VCR/$Vol_{1/24}$ following 24 h of incubation with 10 % fetal bovine serum (FBS). (D) *In vitro* VCR/Vol release from Ps-VCR/$Vol_{1/24}$ under different conditions.

severe long-term side effects [9].

The advancement and approval of small-molecule targeted agents, characterized by enhanced specificity and safety, has changed the therapeutic strategies for ALL and numerous other malignancies [10–13]. Notably, the rational combination of these agents with conventional chemotherapy has the potential to overcome drug resistance and elicit synergistic anticancer effects. Polo-like kinase 1 (PLK1), an oncogene that is overexpressed in a variety of malignancies, including ALL, is reported to be correlated with poor prognosis and resistance to many chemotherapeutics [14–17]. This has greatly propelled the development of PLK1 inhibitors, with volasertib (Vol) emerging as the most extensively studied [18,19]. It has been granted breakthrough therapy by the Food and Drug Administration (FDA) for treating acute myeloid leukemia (AML). The combination of Vol with cytarabine effectively increased the response rate and survival of elderly AML patients unsuitable for intensive chemotherapy [20]. Preclinical studies have demonstrated that PLK1 inhibitors (*e.g.*, Vol) synergize with microtubule-interfering drugs such as vincristine sulfate (VCR), a first-line and standard chemotherapy for ALL, in Ewing sarcoma and rhabdomyosarcoma cells [21,22]. However, the clinical dosage of Vol approaches its maximum tolerated dose, resulting in dose-limiting toxicity, which may exacerbate toxic effects when it is used in combination with chemotherapeutics. Furthermore, the dissimilar pharmacokinetics and biodistributions of different drugs make it difficult to deliver synergistic drug ratios to the tumor site, thus hindering the translation of synergistic effects observed *in vitro* to *in vivo* [23–25].

Herein, we report on a vincristine/volasertib polymersome injection (Ps-VCR/Vol) for delivery at synergistic drug ratios and high-efficiency treatment of ALL *in vivo* (Fig. 1A). Ps-VCR/Vol, with a negatively charged hydrophilic cavity surrounded by a disulfide-crosslinked hydrophobic membrane, effectively and stably loaded VCR/Vol at tailored drug ratios. Interestingly, Ps-VCR/Vol with fixed VCR/Vol ratios not only displayed synergistic antileukemic activity against T-ALL and B-ALL cells but also substantially reduced the leukemia burden in orthotopic ALL mouse models. This reduction in leukemia burden effectively relieved osteolytic bone destruction and significantly prolonged the survival of the mice. In an orthotopic T-ALL patient-derived xenograft (T-ALL PDX) mouse model, Ps-VCR/Vol at a low drug dosage of 0.25/6 mg/kg potently inhibited the proliferation of primary T-ALL cells in mice, leading to a remarkable survival benefit compared with the free

VCR/Vol combination and single-drug polymersomes.

2. Experimental section

2.1. Preparation of vincristine/volasertib polymersomes (Ps-VCR/Vol)

Ps-VCR/Vol was obtained from the one-step self-assembly of poly (ethylene glycol)-*b*-poly(trimethylene carbonate-*co*-dithiolane trimethylene carbonate)-*b*-poly(aspartic acid) (PEG-P(TMC-DTC)-KD_{10}, 5.0-(15.0–2.0)-1.3 kg mol^{-1}), synthesized according to our previous report [26], with concurrent encapsulation of VCR and Vol via electrostatic interactions. The mass feed ratios of VCR to Vol were set to 1:8, 1:16, and 1:32, and the theoretical mass ratio of Vol to polymer was fixed at 1:5. Taking 1:16 as an example, 2.2 mL of Vol solution in dimethyl sulfoxide (DMSO, 20 mg/mL) was mixed with 5.5 mL of PEG-P(TMC-DTC)-KD_{10} solution in DMSO (40 mg/mL) and then injected into an aqueous solution containing 0.55 mL of VCR (5 mg/mL) and 55 mL of 4-(2-hydroxyethyl)-1-piperazine ethanesulfonic acid (HEPES, 5 mM, pH 6.8) at 37 °C with stirring. After overnight incubation at 37 °C, the suspension was dialyzed (MWCO: 3.5 kDa) against HEPES (5 mM, pH 7.4) and concentrated by centrifugal ultrafiltration (Vivaspin, MWCO: 10 kDa) to yield Ps-VCR/Vol with a polymersome concentration of ~10 mg/mL. Ps-VCR and Ps-Vol were prepared similarly, wherein only VCR or Vol was added during the assembly of the polymers.

The size, size distribution, and stability of the polymersomes in the presence of 10 % FBS or diluted with HEPES, phosphate-buffered saline (PBS), water or RPMI-1640 medium supplemented with 10 % FBS were determined via dynamic light scattering (DLS, Zetasizer Nano-ZS, Malvern) with a 633 nm He-Ne laser via back-scattering detection. The VCR content was determined via high-performance liquid chromatography (HPLC) at a wavelength of 298 nm using a mixture of methanol and water (v/vv= 70/30) as the mobile phase. The concentration of Vol was measured with a UV−Vis spectrophotometer (Hitachi UH5300) at a wavelength of 330 nm. The drug loading content (DLC) and drug loading efficiency (DLE) were calculated via the following equations:

$$\text{DLC (wt.\%)} = \frac{\text{mass of loaded VCR or Vol}}{\text{mass of Ps} - \text{VCR/Vol}} \times 100$$

$$\text{DLE (\%)} = \frac{\text{mass of loaded VCR or Vol}}{\text{mass of VCR or Vol in feed}} \times 100$$

VCR/Vol release from Ps-VCR/Vol was investigated under three different conditions, including HEPES at pH 7.4, pH 6.0 and pH 7.4 containing 10 mM glutathione (GSH). The experiments were conducted in triplicate by dialyzing 0.5 mL of Ps-VCR/Vol against 20 mL of release medium. At predetermined timepoints, 5 mL of the medium was sampled, and an equivalent volume of fresh medium was supplemented. The samples were lyophilized, dissolved in 300 μL of a mixture of methanol and water (1:1, v/v), and filtered for HPLC analysis.

2.2. Cellular uptake and the intracellular drug ratio of Ps-VCR/Vol

The cellular uptake of Ps-VCR/Vol was observed via confocal laser scanning microscopy (CLSM) using Did-loaded polymersomes (Ps-Did). In brief, CCRF-CEM cells were seeded on polylysine-pretreated glass slides in 12-well plates (5×10^5 cells/well) to facilitate adhesion, followed by incubation with Ps-Did (Did: 3.45 μM) for 4 h. The cells were then washed with PBS, fixed with 4 % paraformaldehyde solution, and stained with WGA-AF488 and DAPI sequentially. The glass slide was mounted onto a microscope slide with glycerol for CLSM observation.

The intracellular drug ratio of Ps-VCR/Vol in CCRF-CEM cells was quantified after 2–6 h of incubation, and free VCR/Vol was used as a control. CCRF-CEM cells in 6-well plates (2×10^6 cells/well) were incubated with Ps-VCR/$Vol_{1/24}$ or free VCR/$Vol_{1/24}$ for 2, 4 or 6 h at VCR and Vol concentrations of 21 and 500 μg/mL. After incubation, the cells were washed, collected via centrifugation and lysed with 1 % Triton X-100 at 37 °C and 200 rpm for 12 h. The supernatant was then incubated with 10 mM DTT for 12 h and measured by HPLC to quantify the VCR and Vol.

2.3. The synergistic effect of Ps-VCR/Vol in leukemia cells

The synergistic antileukemic effects of Ps-VCR/Vol with different VCR/Vol ratios were evaluated in CCRF-CEM T-ALL and Nalm-6-Luc B-ALL cells via a cell counting kit-8 (CCK-8). The cells were seeded in 96-well plates (2×10^4 cells/well) and incubated with different formulations, including free VCR/$Vol_{1/24}$, Ps-VCR, Ps-Vol, Ps-VCR/$Vol_{1/12}$, Ps-VCR/$Vol_{1/24}$ and Ps-VCR/$Vol_{1/48}$, for 48 h. For the Ps-VCR group, the VCR concentrations ranged from 0.01 to 100 ng/mL, and for the other groups, the Vol concentrations were set from 1 to 50 ng/mL. After incubation, 10 μL of CCK-8 solution was added to each well and further incubated for 4 h. Then, the absorbance at 450 nm in each well was measured with a microplate reader. Cell viability was calculated by comparing the absorbance of cells treated with different drug formulations with that of cells treated with PBS only ($n = 6$). The synergistic effect of Ps-VCR/Vol was assessed by calculating the combination index (CI) via the following equation:

$$CI = \frac{IC_{50,VCR} \text{ for Ps} - \text{VCR/Vol}}{IC_{50,VCR} \text{ for Ps} - \text{VCR}} + \frac{IC_{50,Vol} \text{ for Ps} - \text{VCR/Vol}}{IC_{50,Vol} \text{ for Ps} - \text{Vol}}$$

CI < 1, CI = 1 and CI > 1 indicate synergistic, additive and antagonistic effects, respectively, as clarified in previous reports [27,28].

Human T cells from normal donors were used to investigate the toxicity of Ps-VCR/$Vol_{1/24}$ toward normal cells. T cells were cultured with T-cell-specific medium containing IL-7, IL-10 and TransAct. Activated T cells were seeded in 96-well plates (2×10^4 cells/well) and incubated with Ps-VCR/$Vol_{1/24}$ or free VCR/$Vol_{1/24}$ at final Vol concentrations ranging from 1–100 ng/mL. After 48 h of incubation at 37 °C, the cell viability was determined as described above.

2.4. Cell cycle arrest and cell apoptosis analysis

Both VCR and Vol are known to induce cell cycle arrest and hence cell apoptosis. CCRF-CEM and Nalm-6-Luc cells were used to study the anti-ALL mechanisms of Ps-VCR/Vol in cell cycle arrest and apoptosis. A total of 1.8 mL of cell suspension was added to 6-well plates (4×10^5 cells/well) and incubated with 0.2 mL of PBS, Ps-VCR, Ps-Vol, Ps-VCR/$Vol_{1/24}$, or free VCR/$Vol_{1/24}$. The concentration of Vol was fixed at 10 ng/mL, except for Ps-VCR, which had a VCR concentration of 0.42 ng/mL. After incubation for 24 h, the cells were collected via centrifugation, washed twice with PBS, resuspended in 1 mL of ice-cold PBS, and then slowly added to 4 mL of 95 % ice-cold ethanol in a vortex state. After fixation at 4 °C for 24 h, the cells were washed once with PBS and resuspended in 0.4 mL of a prepared staining solution, which consisted of 0.4 mL of staining buffer, 15 μL of propidium iodide, and 4 μL of RNase A. The cells were subsequently stained for 30 min at 37 °C prior to analysis via flow cytometry.

The apoptosis of ALL cells was studied via an Annexin V-APC/7-AAD double-stained apoptosis kit. Briefly, 1.8 mL of Nalm-6-Luc or CCRF-CEM cells were seeded in 6-well plates (4×10^5 per well), after which 0.2 mL of PBS, Ps-VCR, Ps-Vol, Ps-VCR/$Vol_{1/24}$ or free VCR/$Vol_{1/24}$ was added. The concentration of VCR was 0.21 ng/mL for the Ps-VCR group, and for the other groups, the concentration of Vol was fixed at 5 ng/mL. After 48 h of incubation, the cells were collected via centrifugation, washed twice with PBS, and resuspended in 0.5 mL of binding buffer. Then, 5 μL of Annexin V-APC and 10 μL of 7-AAD were added to each well, and the cells were stained for 5 min at room temperature in the dark for flow cytometry analysis. A minimum of 10,000 cells were collected for each sample.

Table 1
Characterization of Ps-VCR/Vol with different drug ratios.

Polymersomes	Mass ratio of VCR/Vol		VCR		Vol		Size (nm) [c]	PDI[c]
	Theor.	Deter.	DLC (wt. %) [a]	DLE (%)	DLC (wt. %) [b]	DLE (%)		
Ps-VCR	/	/	4.0	80.3	/	/	25.8	0.07
Ps-Vol	/	/	/	/	13.8	80.0	25.1	0.07
Ps-VCR/$Vol_{1/12}$	1/8	1/12.8	1.0	46.2	12.8	74.3	25.9	0.09
Ps-VCR/$Vol_{1/24}$	1/16	1/24.8	0.5	48.8	13.1	75.8	25.8	0.12
Ps-VCR/$Vol_{1/48}$	1/32	1/48.6	0.3	51.5	13.2	76.4	24.9	0.11

a Measured by HPLC, [b] Measured by UV−vis, [c] Measured by DLS.

2.5. In vivo acute toxicity of Ps-VCR/Vol

All the animal experiments were approved by the Animal Care and Use Committee of Soochow University, and all the protocols conformed to the Guide for the Care and Use of Laboratory Animals. Kunming mice (Charles River, 6 weeks old) were used to study the acute toxicity of Ps-VCR/Vol. The mice were randomly assigned to five groups, with each group comprising 5 male and 5 female mice. One group was used as a control, while the remaining groups received a single intravenous injection of HEPES or Ps-VCR/Vol (VCR/Vol: 2/48, 2.5/60 or 3/72 mg/kg) through the tail vein. The status, weight and survival of the mice were monitored continuously for 14 days. Then, another 8 mice were further divided into two groups ($n = 4$, 2 females and 2 males) to receive a single injection of HEPES or Ps-VCR/Vol (2/48 mg/kg). On day 7 after injection, blood was collected for blood routine and blood biochemical analyses.

2.6. In vivo biodistribution

The biodistribution of Cy5-labeled polymersomes (Ps-Cy5) was studied using an orthotopic CCRF-CEM T-ALL model, which was established via the injection of 150 μL of a CCRF-CEM cell suspension (1×10^6 cells) into the tail vein of an NCG mouse (female, 7–8 weeks old; Jiangsu Collective Pharmacies Biotechnology Co., Ltd.). Free Cy5 was used as a control. On day 23 after model establishment, 150 μL of Ps-Cy5 or free Cy5 (Cy5: 0.2 μg per mouse) was injected via the tail vein, and the mice were monitored via an IVIS imaging system at 2 h and 4 h post-injection. Afterwards, the mice were sacrificed, and the forelimbs and hindlimbs were collected for ex vivo imaging.

2.7. Synergistic anti-T-ALL activity of Ps-VCR/Vol in vivo

The synergistic anti-T-ALL activity of Ps-VCR/Vol *in vivo* was first evaluated in an orthotopic CCRF-CEM T-ALL model established via tail vein injection of 5×10^5 CCRF-CEM cells into an NCG mouse. The day of inoculation of CCRF-CEM cells was recorded as day 0. On day 5, the mice were grouped randomly and intravenously administered Ps-VCR/Vol at VCR/Vol dosages of 0.25/6 mg/kg. PBS, Ps-VCR, Ps-Vol and free VCR/Vol were used as controls. The mice were treated every four days for a total of five doses. Each group included 10 mice, of which 6 were used for body weight and survival monitoring, and 4 were used for monitoring leukemia infiltration and performing micro-CT and histological analyses. On days 25 and 39, blood was collected from the eyes of the mice to monitor leukemia progression. For the Ps-Vol, free VCR/Vol and Ps-VCR/Vol groups, 4 mice each were dissected on day 40 to collect the peripheral blood, spleen, liver, lung and bone marrow. The samples were subsequently ground into single-cell suspensions, lysed with ACK lysis buffer, and stained with APC-conjugated anti-human CD45 to determine the leukemia burden via flow cytometry. The leukemia burdens of the PBS- and Ps-VCR-treated mice were measured similarly at their experimental endpoints (day 27 and day 34, respectively) for comparison. Moreover, the hindlimbs and major organs of the mice were collected from each group, fixed with 4 % paraformaldehyde, embedded in paraffin, and stained with hematoxylin and eosin (H&E) for pathological and histological analyses. Furthermore, micro-CT was used to observe the bone structure of each group of mice.

To further corroborate the synergistic anti-T-ALL effect of Ps-VCR/Vol, a patient-derived orthotopic T-ALL PDX model was established in which 200 μL of patient-derived T-ALL cell suspension (2×10^6 cells) was injected into a female NPG mouse (7–8 weeks old; Beijing Vitonda Biotechnology Co., Ltd.) via the tail vein. The day of inoculation was recorded as day 0, and the mice were randomly grouped on day 3, with 6 mice in each group to start treatment. PBS, Ps-VCR, Ps-Vol, Ps-VCR/Vol or free VCR/Vol was injected via the tail vein at the same dose and schedule as those in the orthotopic CCRF-CEM T-ALL model. The body weights and survival of the mice were continuously monitored during and after drug administration, and tumor infiltration in the peripheral blood was examined on days 24, 32, 39, 46 and 52.

2.8. Anti-B-ALL activity of Ps-VCR/Vol in vivo

To further validate the anti-B-ALL effect of Ps-VCR/Vol, an orthotopic Nalm-6-Luc B-ALL model was subsequently established via tail vein injection of 200 μL of Nalm-6-Luc cell suspension (5×10^5 cells) each into 7- to 8-week-old NCG female mice. The day of inoculation was recorded as day 0, and the mice were randomly grouped to administer PBS or Ps-VCR/Vol under the same schedule as above. For each group, 6 mice were used for body weight and survival monitoring, and 4 were used for monitoring leukemia progression via bioluminescence imaging. On day 23, 4 mice in each group were dissected to determine leukemia infiltration in the peripheral blood, spleen, liver, lung and bone marrow via flow cytometry. The collected major organs and hindlimbs were also stained with H&E as described above for histological analysis.

2.9. Statistical analysis

The data were presented as the means ± standard deviations (SDs) and were analyzed with GraphPad Prism 8.0. One-way analysis of variance (ANOVA) with Tukey's post hoc test and Student's *t*-test were used for comparisons between groups. Kaplan−Meier survival curves were constructed and compared via the log-rank Mantel−Cox test. $^*p < 0.05$, $^{**}p < 0.01$, $^{***}p < 0.001$, and $^{****}p < 0.0001$.

3. Results and discussion

3.1. Preparation and characterization of Ps-VCR/Vol

Ps-VCR/Vol was constructed via one-step self-assembly of PEG-P(TMC-DTC)-KD_{10} copolymers with simultaneous VCR and Vol loading through electrostatic interactions (**Fig. S1**). By tuning the theoretical drug ratios, Ps-VCR/Vol with VCR/Vol mass ratios of 1/12.8, 1/24.8, and 1/48.6, respectively, were obtained and defined as Ps-VCR/$Vol_{1/12}$, Ps-VCR/$Vol_{1/24}$ and Ps-VCR/$Vol_{1/48}$, respectively. Given the VCR (0.25 mg/kg) and Vol dosages (6 or 9 mg/kg) that we previously explored for *in vivo* antileukemia studies [29–31], as well as the synergistic ratio of free VCR to Vol observed in Ewing sarcoma cells [21], Ps-VCR/Vol with lower or higher ratios was not tested in this study. Ps-VCR/Vol with different drug contents presented a similar size of *ca.* 26 nm and a

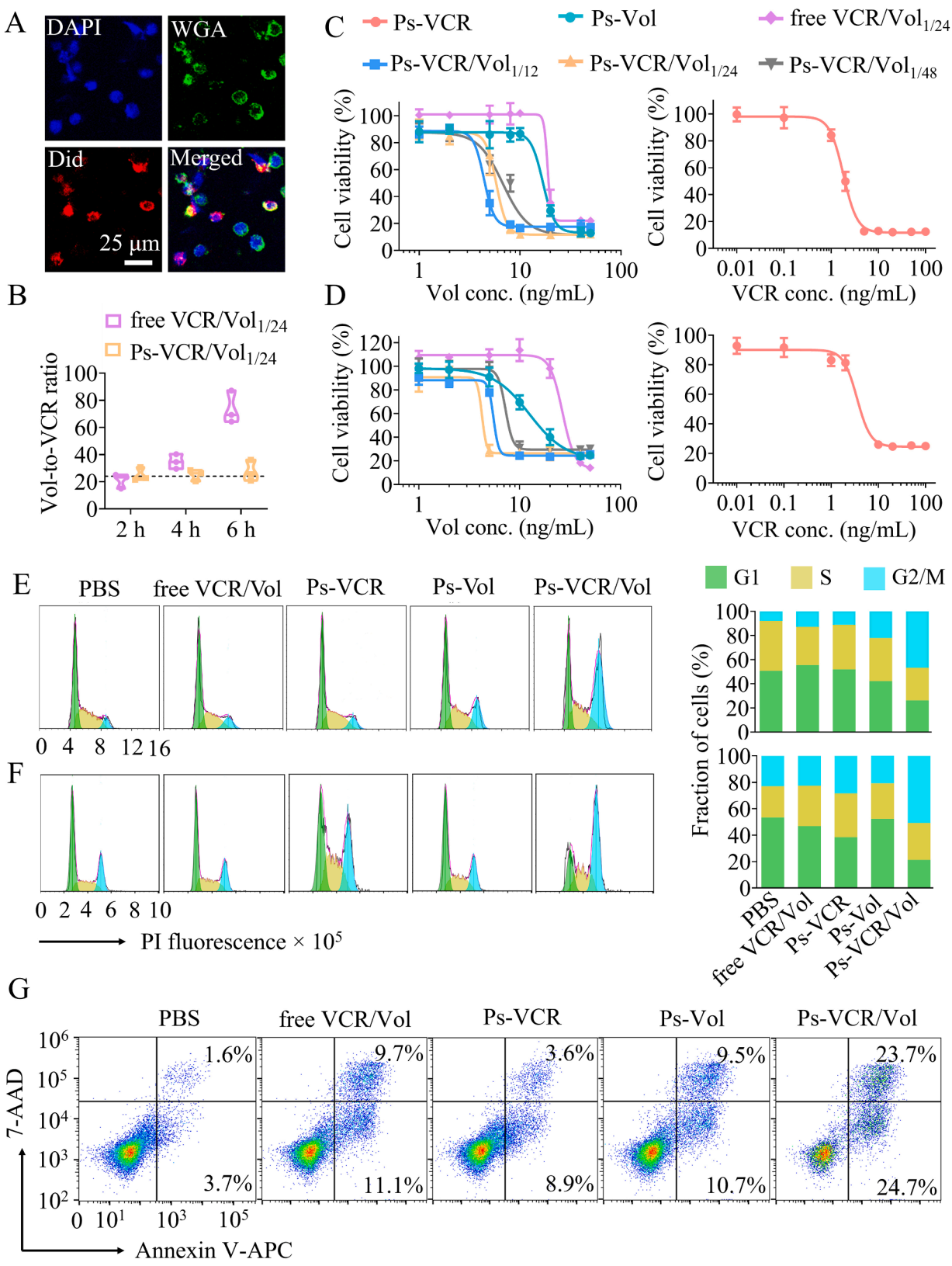

Fig. 2. Cellular uptake and anti-ALL activity of Ps-VCR/Vol with different VCR/Vol ratios. (A) CLSM images of CCRF-CEM cells after 4 h of incubation with Ps-Did. Scale bar is 25 μm. (B) VCR/Vol ratios in CCRF-CEM cells after incubation with free VCR/Vol or Ps-VCR/Vol. Cell viability of (C) CCRF-CEM T-ALL cells and (D) Nalm-6-Luc B-ALL cells following 48 h of incubation with different formulations ($n = 6$). Cell cycle analysis of (E) CCRF-CEM and (F) Nalm-6-Luc cells after treatment with different formulations for 24 h (VCR: 0.42 ng/mL, Vol: 10 ng/mL). (G) Apoptosis of CCRF-CEM cells after 48 h of incubation with different formulations (VCR: 0.21 ng/mL, Vol: 5 ng/mL).

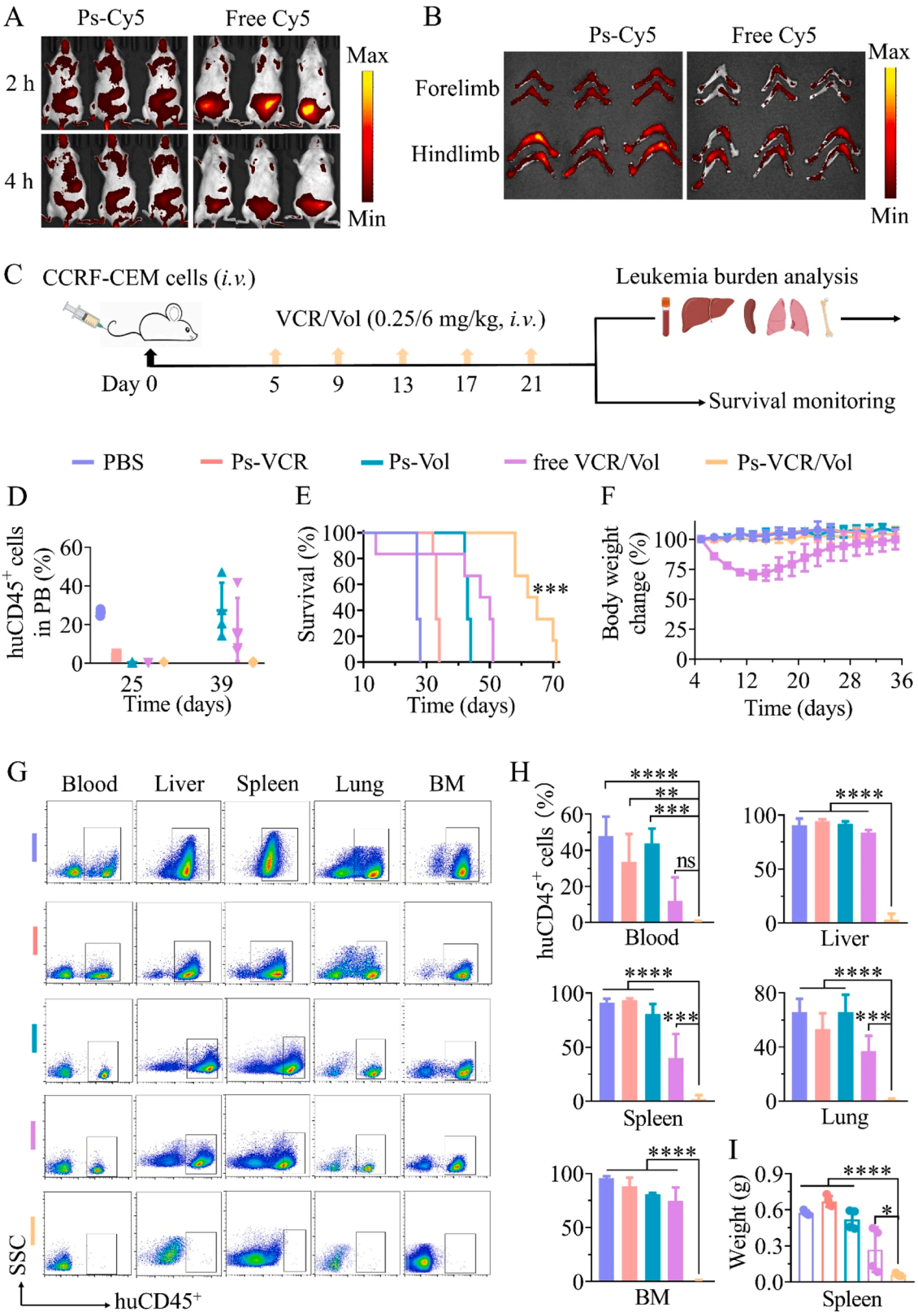

Fig. 3. Biodistribution and synergistic anti-T-ALL activity of Ps-VCR/Vol in mice. (A) *In vivo* fluorescence images of the mice at 2 and 4 h after intravenous injection of Ps-Cy5 or free Cy5. (B) *Ex vivo* fluorescence images of the forelimbs and hindlimbs of the mice at 4 h post-injection ($n = 3$). (C) Schematic showing the treatment and monitoring schedules of orthotopic CCRF-CEM T-ALL-bearing mice. (D) Proportion of CCRF-CEM cells in the peripheral blood of mice in different groups ($n = 4$). (E) Kaplan–Meier survival curves (Ps-VCR/Vol *versus* PBS, Ps-VCR, Ps-Vol, or free VCR/Vol, $^{***}p < 0.001$) and (F) body weight changes of the mice in different groups ($n = 6$). (G) Representative flow cytometry data and (H) quantitative analysis of leukemia burden in different groups ($n = 4$), BM: bone marrow. (I) Weights of spleens isolated from mice in different groups ($n = 4$). $^{*}p < 0.05$, $^{**}p < 0.01$, $^{***}p < 0.001$, $^{****}p < 0.0001$.

narrow size distribution with a polydispersity index (PDI) of ~0.1, similar to those of Ps-VCR and Ps-Vol single-drug formulations (Fig. 1B and Table 1). TEM image further confirmed the spherical and vesicular structure of Ps-VCR/Vol. As a result of the disulfide-crosslinked structure, Ps-VCR/Vol maintained a small size and narrow size distribution after incubation with 10 % FBS for 24 h or high-fold dilutions with HEPES, PBS, water or RPMI-1640 complete medium (Fig. 1C and S2). Moreover, Ps-VCR/Vol displayed <18 % drug leakage after 24 h of incubation at pH 7.4 and 6.0, but nearly completely released VCR and Vol with similar rates after treatment with 10 mM GSH, mimicking the intracellular reductive conditions (Fig. 1D).

3.2. Intracellular drug localization and in vitro anti-ALL activity

To visualize the cellular uptake and localization of drugs in ALL cells, CCRF-CEM cells were incubated with Ps-Did and observed via CLSM. As shown in Fig. 2A, Ps-Did was efficiently internalized in CCRF-CEM cells, resulting in strong Did fluorescence. A controllable intracellular drug ratio is important for inducing synergistic antitumor effects. Ps-VCR/Vol maintained a relatively stable intracellular VCR/Vol mass ratio of close to 1:24 within 6 h of incubation, which was in sharp contrast to the free VCR/Vol, with the ratio deviating to 1:87 (Fig. 2B). The synergistic anti-ALL effect of Ps-VCR/Vol with different VCR/Vol ratios was investigated using CCRF-CEM T-ALL and Nalm-6-Luc B-ALL cells. As shown in Fig. 2C and **Table S1**, Ps-VCR/Vol with VCR/Vol mass ratios of 1:12, 1:24 and 1:48 potently inhibited the proliferation of CCRF-CEM T-ALL cells and displayed a similar and strong synergistic effect, with CI values of *ca.* 0.46. For example, Ps-VCR/$Vol_{1/24}$ presented IC_{50} values of 0.24/5.69 ng/mL for VCR and Vol, which were 8.1- and 3.0-fold lower than those of Ps-VCR (1.94 ng/mL) and Ps-Vol (16.98 ng/mL), respectively. In addition, Ps-VCR/$Vol_{1/24}$ had 3.3-fold greater anti-T-ALL activity than free VCR/$Vol_{1/24}$ did, likely due to its controllable intracellular drug ratio and different cellular uptake pathways, as previously reported for dual-drug formulations [32–34]. Similarly, Ps-VCR/Vol with different VCR/Vol ratios (1:12 to 1:48) also exhibited strong synergy in Nalm-6-Luc B-ALL cells, with CI values ranging from 0.32–0.54. Ps-VCR/$Vol_{1/24}$ was the most synergistic, with an IC_{50} of 0.17/4.16 ng/mL (VCR/Vol), which was 23.4-, 3.6- and 6.9-fold lower than those of Ps-VCR (3.98 ng/mL), Ps-Vol (15.14 ng/mL) and free VCR/$Vol_{1/24}$ (1.17/28.18 ng/mL), respectively (Fig. 2D and **Table S1**). Hereinafter, Ps-VCR/$Vol_{1/24}$ with a fixed VCR/Vol ratio of 1:24 was used and denoted Ps-VCR/Vol unless otherwise specified. Free VCR/Vol at the same ratio was used as a control. For normal human T cells, Ps-VCR/Vol showed negligible toxicity, with a cell viability of over 90 %, even at VCR/Vol concentrations as high as 5/100 ng/mL (**Fig. S3**). However, the viability of T cells decreased to ~52 % after incubation with free VCR/Vol at a lower concentration of 2.5/50 ng/mL, suggesting that drug coloading improved their safety.

VCR is a microtubule-destabilizing compound that interferes with mitosis and arrests the cell cycle at the M phase, leading to cell apoptosis [35–37]. Vol is reported to inhibit PLK1, a key regulator of the cell cycle, thus disrupting spindle formation and inducing G2/M cell cycle arrest and apoptosis [38,39]. Therefore, the synergistic anti-ALL effect of Ps-VCR/Vol was further explored via cell cycle and apoptosis analyses. Ps-VCR/Vol effectively induced G2/M phase arrest in CCRF-CEM cells after 24 h of incubation, and the proportion of cells in the G2/M phase significantly increased from 8.0 % (in the PBS group) to 46.7 % and was obviously higher than that in the Ps-VCR (11.2 %) and Ps-Vol (22.1 %) groups (Fig. 2E). However, free VCR/Vol induced limited cell cycle arrest, with 12.9 % of the cells in the G2/M phase, which was 3.6-fold lower than that of Ps-VCR/Vol. Consistently, treatment with Ps-VCR/Vol increased the percentage of G2/M arrest of Nalm-6-Luc cells to 50.8 %, which was significantly greater than that in the Ps-VCR (28.4 %), Ps-Vol (22.8 %), and free VCR/Vol (22.6 %) groups (Fig. 2F).

In line with the cell cycle arrest data, the results of the apoptosis analysis revealed that Ps-VCR/Vol caused the most significant apoptosis in CCRF-CEM cells, with 48.4 % of the cells undergoing early- and late-stage apoptosis, which was obviously greater than those of Ps-VCR (12.5 %), Ps-Vol (20.2 %) and free VCR/Vol (20.8 %) (Fig. 2G). Similarly, Ps-VCR/Vol also had the strongest proapoptotic effect on Nalm-6-Luc cells, with an apoptosis rate of 80.8 %, which was 5.8-fold higher than that of free VCR/Vol (14.0 %) (**Fig. S4**). Taken together, these results corroborate that Ps-VCR/Vol can synergistically induce the arrest of ALL cells in the G2/M phase, thus promoting cell apoptosis and enhancing the inhibition of ALL cells.

3.3. In vivo acute toxicity and anti-T-ALL activity of Ps-VCR/Vol

In vivo acute toxicity studies in Kunming mice demonstrated that Ps-VCR/Vol had good tolerability at a VCR/Vol dose of 2/48 mg/kg. The blood routine and biochemical parameters of these mice were comparable to those of untreated mice, and their weights at the end of monitoring were similar to those of the controls, leading to a survival rate of 100 % (**Fig. S5**). When the dosage was further increased to 2.5/60 or 3/72 mg/kg, the mortality rate increased to 50 % or 100 %, respectively, during the 14-day observation period. To investigate the *in vivo* performance of Ps-VCR/Vol, an orthotopic CCRF-CEM T-ALL mouse model was first established via the tail vein injection of CCRF-CEM cells into each NCG mouse. The biodistribution of Ps-Cy5 was studied via *in vivo* and *ex vivo* fluorescence imaging when the CCRF-CEM T-ALL mouse model manifested clear signs of illness. As shown in Fig. 3A, intravenously injected Ps-Cy5 rapidly accumulated in the limbs of the mice, the primary site of ALL, within 2 h and maintained consistent Cy5 fluorescence levels at 4 h post-injection. However, free Cy5 showed obviously lower accumulation in the limbs of the mice at 2 h, and this accumulation further decreased at 4 h, indicating its rapid metabolism. *Ex vivo* fluorescence images further confirmed the greater accumulation of Ps-Cy5 than free Cy5 in the forelimbs and hindlimbs of the mice (Fig. 3B). Anti-T-ALL treatment was started on day 5 post-injection of CCRF-CEM cells via intravenous injection of Ps-VCR/Vol, Ps-VCR, Ps-Vol or free VCR/Vol at VCR/Vol dosages of 0.25/6 mg/kg (Fig. 3C). The PBS-treated control mice displayed rapid proliferation of CCRF-CEM cells and a substantial T-ALL burden in the peripheral blood (26.3 % on day 25), along with hindlimb paralysis, hair lusterlessness and death (Fig. 3D and S6). In contrast, Ps-VCR/Vol treatment significantly inhibited T-ALL progression, and there were nearly undetectable CCRF-CEM cells in the peripheral blood even on day 39. Although the mice in the Ps-Vol and free VCR/Vol groups presented negligible T-ALL burdens in the blood on day 25, they presented fast leukemia growth, with the proportion of CCRF-CEM cells increasing to 27.4 % and 17.5 % on day 39, which were 54- and 35-fold higher than those in the Ps-VCR/Vol group, respectively. However, Ps-VCR only slightly delayed the progression of T-ALL, with ~4.0 % CCRF-CEM cells in the peripheral blood on day 25. Accordingly, Ps-VCR/Vol treatment effectively prolonged the median survival of the mice to 63.5 days, which was 2.4-fold as long as that of the PBS group (27 days) and significantly longer than that of the Ps-VCR (33 days), Ps-Vol (43 days) and free VCR/Vol (48.5 days) groups (***$p < 0.001$) (Fig. 3E). Moreover, in contrast to free VCR/Vol, which exhibited severe systemic toxicity and caused *ca.* 25 % weight loss in the mice, Ps-VCR/Vol was well tolerated, and the weight of the mice was comparable to that of the PBS group (Fig. 3F). The enhanced efficacy and safety of Ps-VCR/Vol might be due to its improved pharmacokinetics and biodistribution, for example, bone marrow accumulation at synergistic drug ratios, which has been observed for the clinically approved liposomal formulation CPX-351 and venetoclax/sorafenib-coloaded micelles in AML models [40,41]

In addition to infiltrating the bone marrow and blood, T-ALL cells usually infiltrate extramedullary organs such as the liver and spleen, resulting in hepatosplenomegaly [42,43]. The infiltration of CCRF-CEM T-ALL cells into different sites of mice after treatment with Ps-VCR/Vol, Ps-Vol, or free VCR/Vol was analyzed by flow cytometry on day 40 and compared with that of the PBS and Ps-VCR groups at their experimental

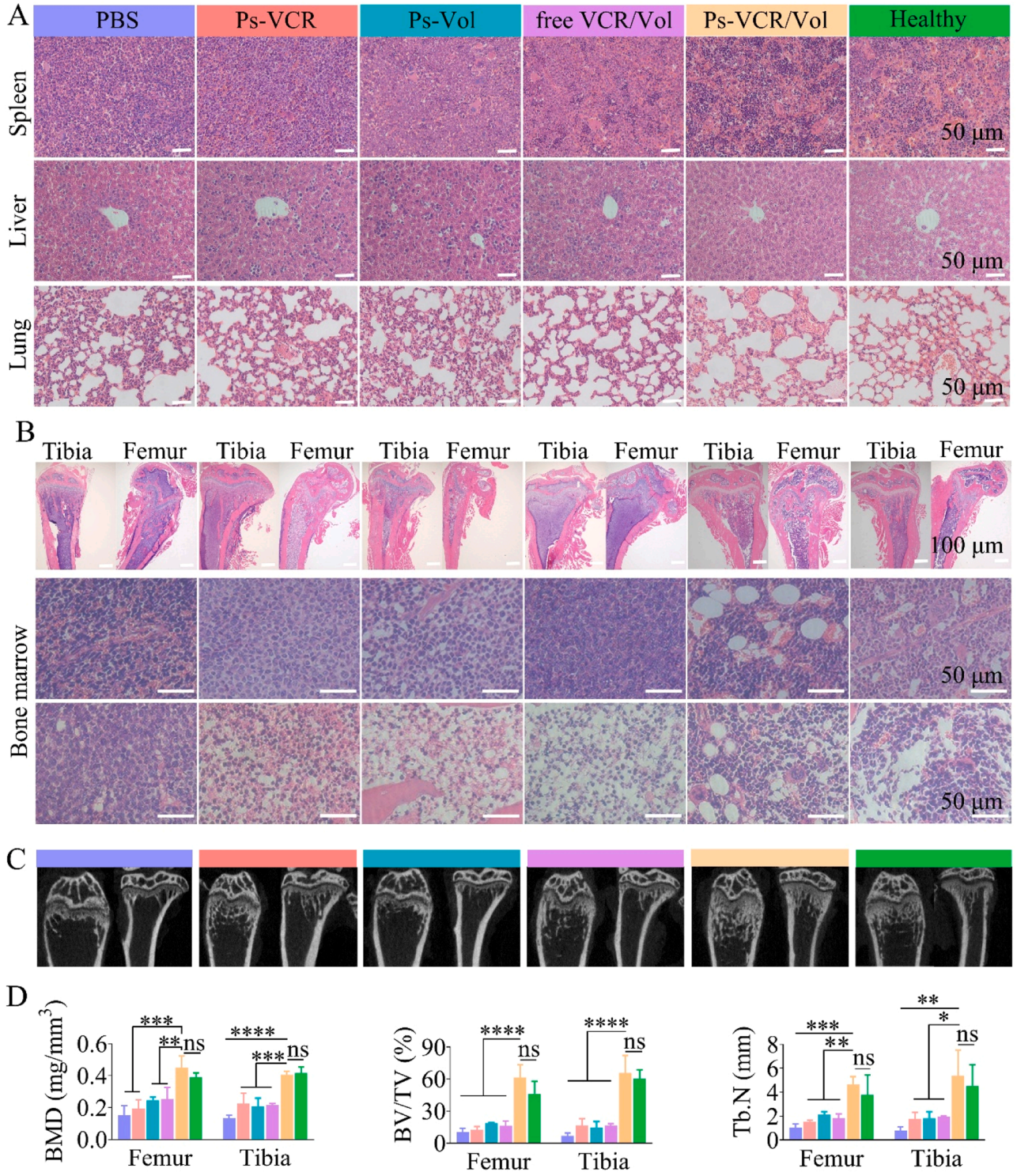

Fig. 4. T-ALL infiltration and osteolysis in orthotopic CCRF-CEM T-ALL-bearing mice following different treatments. H&E-stained images of (A) the spleen, liver, lung, and (B) hindlimbs collected from different groups. Scale bars: 100 μm. (C) Micro-CT images of representative murine femurs and tibias and (D) quantitative analysis of the data ($n = 3$). One-way ANOVA: $^{*}p < 0.05$, $^{**}p < 0.01$, $^{***}p < 0.001$, $^{****}p < 0.0001$.

endpoints. As shown in Fig. 3G, H, the PBS-treated mice suffered a severe T-ALL burden, with >90 % CCRF-CEM cells in the bone marrow, spleen and liver, as well as 65.7 % in the lung and 47.8 % in the peripheral blood, which was in line with previous reports [44,45]. Compared with those in the PBS group, the T-ALL burdens in different tissues of the mice in the Ps-VCR and Ps-Vol groups were comparable. Free VCR/Vol treatment reduced the T-ALL burden in the peripheral blood and lungs of the mice, but had a negligible effect on those in the bone marrow, spleen and liver, with 74.5 %−86.6 % CCRF-CEM cells remaining. In contrast, Ps-VCR/Vol almost completely depleted the T-ALL burden in different tissues, with only 0.4–1.9 % CCRF-CEM cells, which was markedly lower than that in all the other control groups. For instance, the proportion of CCRF-CEM cells was only 0.8 % at the primary T-ALL site (bone marrow), which was 90–115-fold lower than that in the PBS, Ps-VCR, Ps-Vol and free VCR/Vol groups. As a result of the potent inhibition of T-ALL progression and infiltration, Ps-VCR/Vol

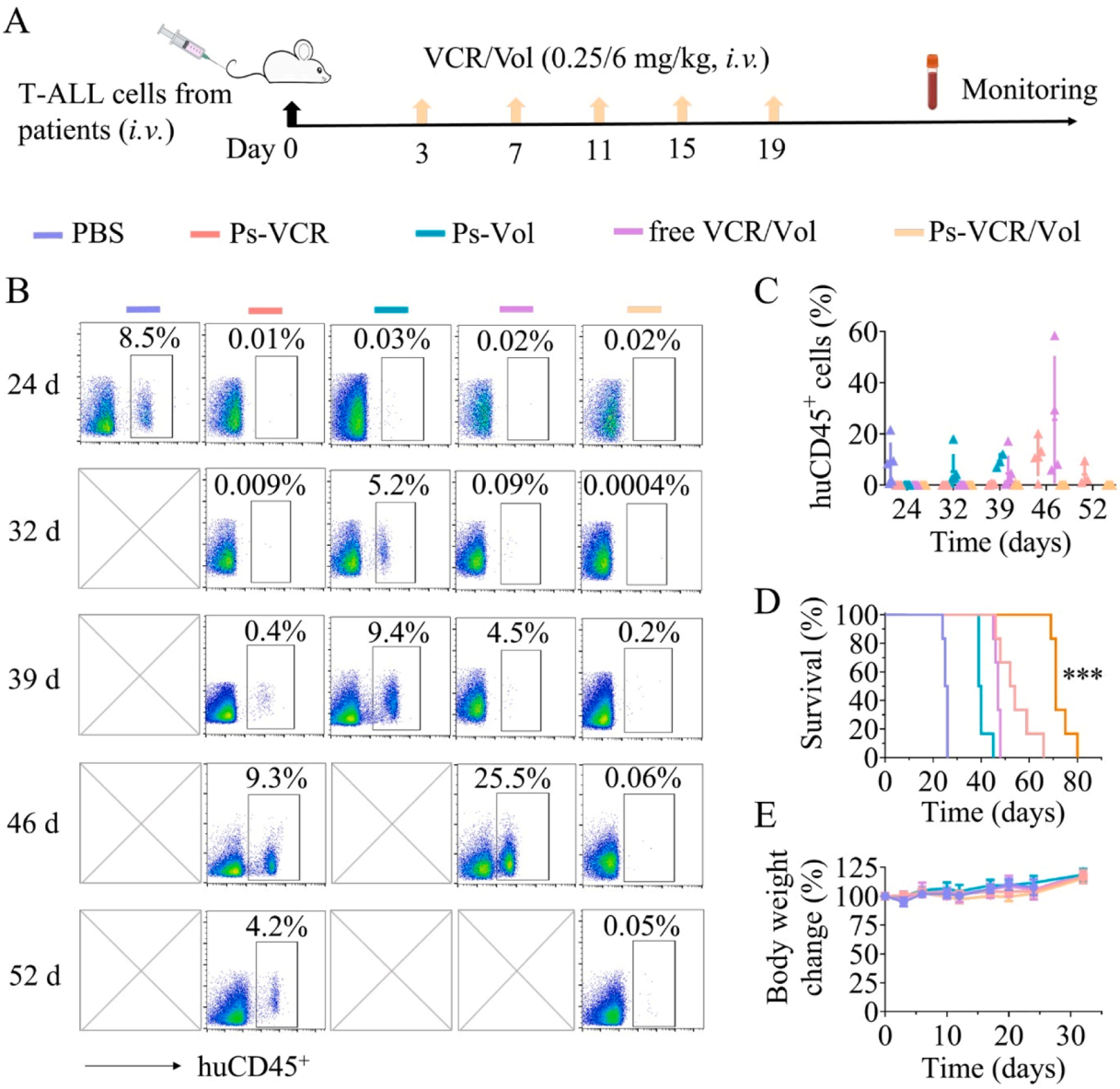

Fig. 5. Anti-T-ALL activity of Ps-VCR/Vol in an orthotopic T-ALL PDX model. (A) Model establishment, treatment and monitoring schemes. (B) Representative flow cytometry pattern and (C) quantitative analysis showing the proliferation of T-ALL cells in the peripheral blood of mice in different groups ($n = 3$). (D) Kaplan–Meier survival curves (Ps-VCR/Vol *versus* Ps-VCR, Ps-Vol, or free VCR/Vol, ***$p < 0.001$) and (E) body weight changes of the mice after different treatments ($n = 6$).

effectively relieved splenomegaly in the mice, resulting in an average spleen weight of 61 mg, which was significantly lower than that in the PBS group (576.1 mg) and only 1/11–1/4 the weight of the other control groups (Fig. 3I).

H&E-stained images provided further evidence that Ps-VCR/Vol-treated mice had undetectable T-ALL cells in major organs and bone marrow, which presented normal histomorphology and was comparable to that of healthy mice (Fig. 4A, B and S7). However, for the PBS-, Ps-VCR-, Ps-Vol- or free VCR/Vol-treated mice, a massive T-ALL burden was detected in the spleen, liver, lung and hindlimbs. The abnormal proliferation of T-ALL cells in the bone marrow generally causes bone marrow failure and impairs hematopoietic function, which are typical symptoms in T-ALL patients [46]. As expected, Ps-VCR/Vol treatment effectively relieved hematopoietic dysfunction, resulting in abundant hematopoietic cells in the marrow cavity, which was in sharp contrast to all the other control groups, which presented obvious loss of hematopoietic cells and/or infiltration of T-ALL cells (Fig. 4B). The massive proliferation of leukemia cells in the bone marrow is also known to induce osteolytic destruction, a symptom that is particularly common in patients with ALL [47]. Therefore, the bone structure of the femur and tibia collected from each group of mice was further analyzed via micro-CT. The mice in the PBS group exhibited severe osteolysis in the femur and tibia with a significant loss of trabeculae, which was substantially ameliorated in the Ps-VCR/Vol group, and the bone structure resembled that of healthy mice (Fig. 4C). This is in contrast to the Ps-VCR, Ps-Vol and free VCR/Vol treatments, which led to only partial alleviation. A quantitative assessment further demonstrated that the femur and tibia parameters of Ps-VCR/Vol-treated mice were comparable to those of healthy mice; specifically, their bone mineral density (BMD), bone volume fraction (BV/TV), trabecular number (Tb.N), bone surface area and trabecular thickness were significantly greater than those of the other groups (Fig. 4D and S8).

To further corroborate the synergistic anti-T-ALL activity of Ps-VCR/Vol, an orthotopic T-ALL PDX model was established via the tail vein injection of 2×10^6 patient-derived T-ALL cells into each mouse. On day 3 post inoculation, the mice were treated with different formulations via

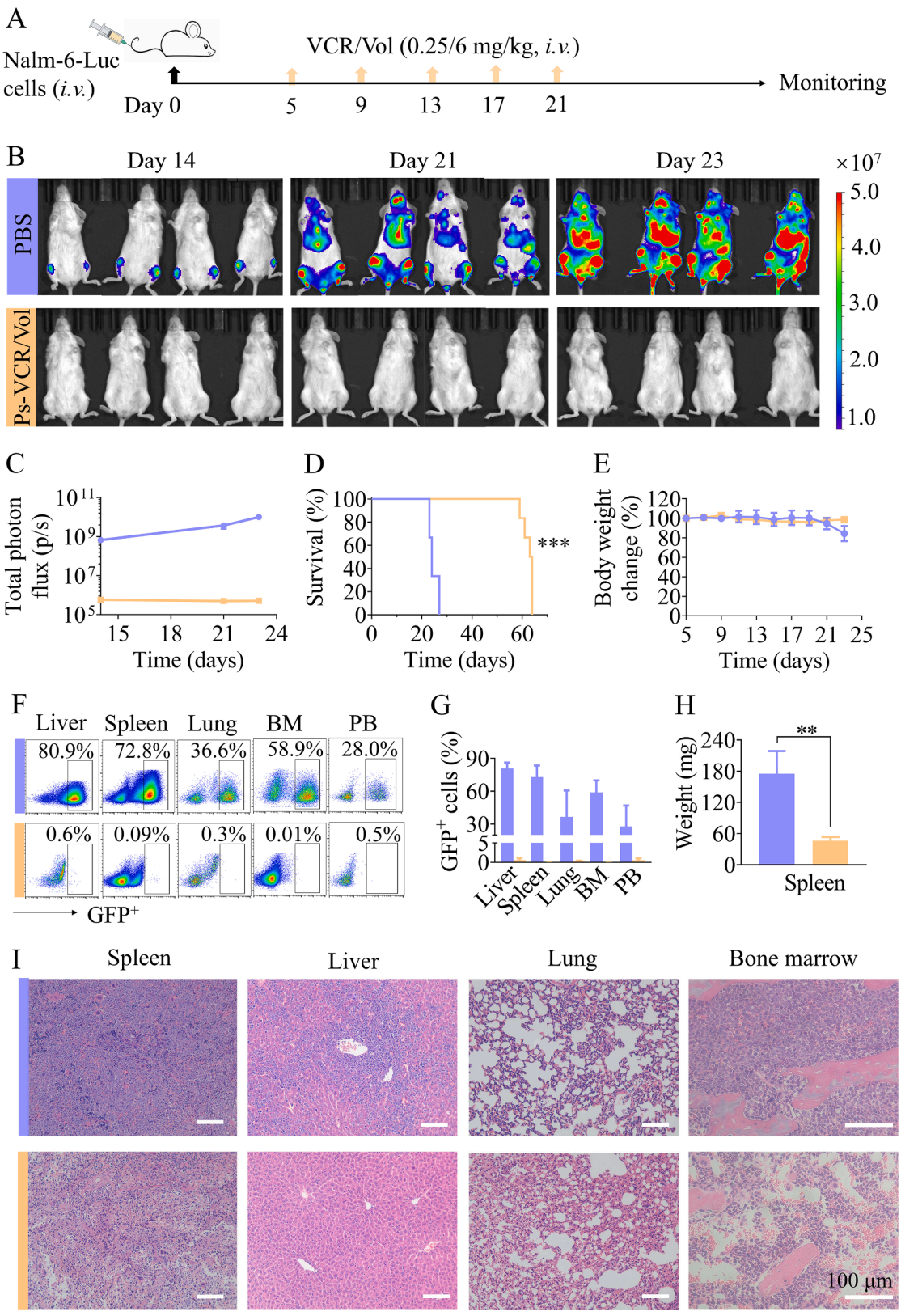

Fig. 6. Therapeutic effect of Ps-VCR/Vol in orthotopic Nalm-6-Luc B-ALL-bearing mice. (A) Model establishment and treatment schemes. (B) Bioluminescence images, (C) quantitative bioluminescence signal analysis ($n = 4$), (D) Kaplan–Meier survival curves ($n = 6$, $^{***}p < 0.001$) and (E) body weight changes ($n = 6$) of the mice after treatment with Ps-VCR/Vol or PBS. (F) Scatter plot and (G) quantitative analysis of the number of Nalm-6-Luc cells in the liver, spleen, lung, bone marrow (BM) and peripheral blood (PB) of Ps-VCR/Vol- or PBS-treated mice ($n = 4$). (H) Weights of the spleens of the mice in the different groups ($n = 4$). (I) H&E-stained images of the liver, spleen, lung, and bone marrow from PBS- or Ps-VCR/Vol-treated mice. Scale bars: 100 μm.

the same scheme as that used for the orthotopic CCRF-CEM model (Fig. 5A). Consistently, Ps-VCR/Vol also completely inhibited T-ALL progression in the peripheral blood of the mice, as reflected by the absence of T-ALL cells during the observation period of 52 days, which was in sharp contrast to the 8.5 % T-ALL cells in the PBS group on day 24 and the 8.9–25.5 % T-ALL cells in the other groups on days 32–46 (Fig. 5B, C). As a result, Ps-VCR/Vol markedly prolonged the median survival of the mice to 71 days, which was 2.8-fold as long as that in the PBS group and significantly greater than that in the Ps-VCR (53 days, $^{***}p < 0.001$), Ps-Vol (39.5 days, $^{***}p < 0.001$) and free VCR/Vol (47 days, $^{***}p < 0.001$) groups (Fig. 5D). The weight of the mice in all the groups steadily increased (Fig. 5E). Taken together, these results demonstrated that Ps-VCR/Vol synergistically inhibited T-ALL progression *in vivo*, thus blocking T-ALL invasion into major organs and significantly prolonging the survival of the mice.

3.4. Anti-B-ALL activity of Ps-VCR/Vol in vivo

To assess the anti-B-ALL activity of Ps-VCR/Vol, an orthotopic B-ALL mouse model was established via intravenous injection of 5×10^5 Nalm-6-Luc cells into each mouse, which was subsequently treated with Ps-VCR/Vol via the same scheme as the CCRF-CEM T-ALL model (Fig. 6A). As shown in Fig. 6B, C, the bioluminescence signal from B-ALL cells spread throughout the body of the PBS-treated mice and increased to $\sim 10^{10}$ p/s on day 23 post inoculation; however, it was completely depleted in the Ps-VCR/Vol group, resulting in a four-order-of-magnitude low background signal (5.2×10^5 p/s). Consequently, Ps-VCR/Vol significantly prolonged the median survival of the mice to 63.5 days, which was 2.6-fold as long as that in the PBS group (MST: 24 days, $^{***}p < 0.001$) (Fig. 6D), superior to CD19-CAR-T cell therapy [48, 49]. Notably, Ps-VCR/Vol showed no substantial toxicity, and the weights of the mice were similar to those of the PBS-treated mice (Fig. 6E). Leukemia burden analysis further evidenced the potent anti-B-ALL activity of Ps-VCR/Vol, where Nalm-6-Luc B-ALL cells in the liver, spleen, lung, bone marrow and blood were all reduced to almost undetectable levels (< 0.6 %), and splenomegaly was effectively relieved, with a 3.8-fold lower spleen weight (Fig. 6F-H). H&E-stained images also verified that the major organs and bone marrow of Ps-VCR/Vol-treated mice had normal histomorphology, which was in sharp contrast to that of the PBS group with severe infiltration of B-ALL cells (Fig. 6I and Fig. S9). Taken together, Ps-VCR/Vol is a potent strategy applicable for both T-ALL and B-ALL treatment.

4 Conclusion

In summary, we have facilely prepared vincristine/volasertib polymersomes (Ps-VCR/Vol) with small sizes and tunable drug ratios, which enable highly synergistic inhibition of both T-ALL and B-ALL in mice. Ps-VCR/Vol exhibits strong synergy in different ALL cells and effectively inhibits leukemia progression, leading to a significant survival benefit in both cell line- and patient-derived orthotopic ALL models, which is superior to that of single-drug polymersomes and free VCR/Vol. Notably, Ps-VCR/Vol with a straightforward fabrication process not only augments the synergistic effects of VCR and Vol via codelivery but also mitigates systemic toxicity. This approach may provide a combination therapy for ALL treatment that is both safe and potent.

CRediT authorship contribution statement

Qing Deng: Writing – original draft, Investigation, Formal analysis, Data curation. **Shujing Yue:** Methodology, Investigation, Formal analysis. **Fengtao You:** Methodology, Investigation. **Zhenzhen Zhai:** Investigation, Data curation. **Huanli Sun:** Writing – review & editing, Supervision, Funding acquisition, Conceptualization. **Lanlan Liang:** Investigation. **Chenming Li:** Validation. **Lin Yang:** Supervision, Methodology. **Zhiyuan Zhong:** Writing – review & editing, Supervision, Funding acquisition, Conceptualization.

Declaration of competing interest

The authors declare that they have no known competing financial interests or personal relationships that could have appeared to influence the work reported in this paper.

Acknowledgements

This work was supported by the National Natural Science Foundation of China (52273251, 52473264, and 52233007) and the Natural Science Foundation of the Jiangsu Higher Education Institutions of China (21KJA150007).

Supplementary materials

Supplementary material associated with this article can be found, in the online version, at doi:10.1016/j.actbio.2025.05.041.

References

[1] L. Pagliaro, S.J. Chen, D. Herranz, C. Mecucci, C.J. Harrison, C.G. Mullighan, M. Zhang, Z. Chen, N. Boissel, S.S. Winter, G. Roti, Acute lymphoblastic leukaemia, Nat. Rev. Dis. Primers 10 (2024) 41.
[2] B. Shah, R.J. Mattison, R. Abboud, P. Abdelmessieh, I. Aldoss, P.W. Burke, D. J. DeAngelo, S. Dinner, A.T. Fathi, J. Gauthier, M. Haddadin, N. Jain, B. Jonas, S. Kirby, M. Liedtke, M. Litzow, A. Logan, M. Long, S. Luger, J.K. Mangan, S. Massaro, W. May, O. Oluwole, J. Park, A. Przespolewski, S. Rangaraju, C. Saygin, M. Schwartz, P. Shami, B. Tomlinson, J. Webster, A. Awotiwon, K. Stehman, Acute lymphoblastic leukemia, version 2.2024, NCCN clinical practice guidelines in oncology, J. Natl. Compr. Canc. Netw. 22 (2024) 563–576.
[3] F. Malard, M. Mohty, Acute lymphoblastic leukemia, Lancet 395 (2020) 1146–1162.
[4] S.W. Brady, K.G. Roberts, Z. Gu, L. Shi, S. Pounds, D. Pei, C. Cheng, Y. Dai, M. Devidas, C. Qu, A.N. Hill, D. Payne-Turner, X. Ma, I. Iacobucci, P. Baviskar, L. Wei, S. Arunachalam, K. Hagiwara, Y. Liu, D.A. Flasch, Y. Liu, M. Parker, X. Chen, A.H. Elsayed, O. Pathak, Y. Li, Y. Fan, J.R. Michael, M. Rusch, M. R. Wilkinson, S. Foy, D.J. Hedges, S. Newman, X. Zhou, J. Wang, C. Reilly, E. Sioson, S.V. Rice, V.P. Loyola, G. Wu, E. Rampersaud, S.C. Reshmi, J. Gastier-Foster, J.M. Guidry Auvil, P. Gesuwan, M.A. Smith, N. Winick, A.J. Carroll, N. A. Heerema, R.C. Harvey, C.L. Willman, E. Larsen, E.A. Raetz, M.J. Borowitz, B. L. Wood, W.L. Carroll, P.A. Zweidler-McKay, K.R. Rabin, L.A. Mattano, K. W. Maloney, S.S. Winter, M.J. Burke, W. Salzer, K.P. Dunsmore, A.L. Angiolillo, K. R. Crews, J.R. Downing, S. Jeha, C.-H. Pui, W.E. Evans, J.J. Yang, M.V. Relling, D. S. Gerhard, M.L. Loh, S.P. Hunger, J. Zhang, C.G. Mullighan, The genomic landscape of pediatric acute lymphoblastic leukemia, Nat. Genet. 54 (2022) 1376–1389.
[5] E. Jabbour, N.J. Short, N. Jain, F.G. Haddad, M.A. Welch, F. Ravandi, H. Kantarjian, The evolution of acute lymphoblastic leukemia research and therapy at md anderson over four decades, J. Hematol. Oncol. 16 (2023) 22.
[6] D. Hoelzer, Chemotherapy-free treatment - a new era in acute lymphoblastic leukemia? New. Engl. J. Med. 383 (2020) 1673–1674.
[7] N. Shukla, M.L. Sulis, Blinatumomab for treatment of children with high-risk relapsed B-cell acute lymphoblastic leukemia, JAMA 325 (2021) 830–832.
[8] X. Xie, Y. Hu, T. Ye, Y. Chen, L. Zhou, F. Li, X. Xi, S. Wang, Y. He, X. Gao, W. Wei, G. Ma, Y. Li, Therapeutic vaccination against leukemia via the sustained release of co-encapsulated anti-PD-1 and a leukemia-associated antigen, Nat. Biomed. Eng. 5 (2021) 414–428.
[9] M. Greaves, A causal mechanism for childhood acute lymphoblastic leukaemia, Nat. Rev. Cancer 18 (2018) 471–484.
[10] Y.T. Lee, Y.J. Tan, C.E. Oon, Molecular targeted therapy: treating cancer with specificity, Eur. J. Pharmacol. 834 (2018) 188–196.
[11] R. Santos, O. Ursu, A. Gaulton, A.P. Bento, R.S. Donadi, C.G. Bologa, A. Karlsson, B. Al-Lazikani, A. Hersey, T.I. Oprea, J.P. Overington, A comprehensive map of molecular drug targets, Nat. Rev. Drug Discov. 16 (2017) 19–34.
[12] T.H. Tran, S.P. Hunger, The genomic landscape of pediatric acute lymphoblastic leukemia and precision medicine opportunities, Semin. Cancer Biol. 84 (2022) 144–152.
[13] H. Inaba, C.G. Mullighan, Pediatric acute lymphoblastic leukemia, Haematologica 105 (2020) 2524–2539.
[14] S. Iliaki, R. Beyaert, I.S. Afonina, Polo-like kinase 1 (PLK1) signaling in cancer and beyond, Biochem. Pharmacol. 193 (2021) 114747.
[15] T. Otto, P. Sicinski, Cell cycle proteins as promising targets in cancer therapy, Nat. Rev. Cancer 17 (2017) 93–115.
[16] K. Strebhardt, Multifaceted polo-like kinases: drug targets and antitargets for cancer therapy, Nat. Rev. Drug Discov. 9 (2010) 643–660.

[17] Z. Wang, S. Zhao, J. shi, F. Meng, J. Yuan, Z. Zhong, Folate-mediated targeted PLK1 inhibition therapy for ovarian cancer: a comparative study of molecular inhibitors and siRNA therapeutics, Acta Biomater. 138 (2022) 443–452.
[18] J. Van den Bossche, F. Lardon, V. Deschoolmeester, I. De Pauw, J.B. Vermorken, P. Specenier, P. Pauwels, M. Peeters, A. Wouters, Spotlight on volasertib: preclinical and clinical evaluation of a promising PLK1 inhibitor, Med. Res. Rev. 36 (2016) 749–786.
[19] J. Zhang, L. Zhang, J. Wang, L. Ouyang, Y. Wang, Polo-like kinase 1 inhibitors in human cancer therapy: development and therapeutic potential, J. Med. Chem. 65 (2022) 10133–10160.
[20] H. Dohner, M. Lubbert, W. Fiedler, L. Fouillard, A. Haaland, J.M. Brandwein, S. Lepretre, O. Reman, P. Turlure, O.G. Ottmann, C. Muller-Tidow, A. Kramer, E. Raffoux, K. Dohner, R.F. Schlenk, F. Voss, T. Taube, H. Fritsch, J. Maertens, Randomized, phase 2 trial of low-dose cytarabine with or without volasertib in AML patients not suitable for induction therapy, Blood 124 (2014) 1426–1433.
[21] L.M. Weiß, M. Hugle, S. Romero, S. Fulda, Synergistic induction of apoptosis by a polo-like kinase 1 inhibitor and microtubule-interfering drugs in ewing sarcoma cells, Int. J. Cancer 138 (2016) 497–506.
[22] M. Hugle, K. Belz, S. Fulda, Identification of synthetic lethality of PLK1 inhibition and microtubule-destabilizing drugs, Cell Death Differ. 22 (2015) 1946–1956.
[23] S. Rawal, M.M. Patel, Threatening cancer with nanoparticle aided combination oncotherapy, J. Control. Release 301 (2019) 76–109.
[24] A. Detappe, H.V.T. Nguyen, Y. Jiang, M.P. Agius, W. Wang, C. Mathieu, N.K. Su, S. L. Kristufek, D.J. Lundberg, S. Bhagchandani, I.M. Ghobrial, P.P. Ghoroghchian, J. A. Johnson, Molecular bottlebrush prodrugs as mono- and triplex combination therapies for multiple myeloma, Nat. Nanotechnol. 18 (2023) 184–192.
[25] R.X. Zhang, H.L. Wong, H.Y. Xue, J.Y. Eoh, X.Y. Wu, Nanomedicine of synergistic drug combinations for cancer therapy – strategies and perspectives, J. Control. Release 240 (2016) 489–503.
[26] N. Yu, Y. Zhang, J. Li, W. Gu, S. Yue, B. Li, F. Meng, H. Sun, R. Haag, J. Yuan, Z. Zhong, Daratumumab immunopolymersome-enabled safe and CD38-targeted chemotherapy and depletion of multiple myeloma, Adv. Mater. 33 (2021) 2007787.
[27] T.-C. Chou, Theoretical basis, experimental design, and computerized simulation of synergism and antagonism in drug combination studies, Pharmacol. Rev. 58 (2006) 621–681.
[28] M. Wu, Y. Wang, D. Yang, Y. Gong, F. Rao, R. Liu, Y. Danna, J. Li, J. Fan, J. Chen, W. Zhang, Q. Zhan, A PLK1 kinase inhibitor enhances the chemosensitivity of cisplatin by inducing pyroptosis in oesophageal squamous cell carcinoma, EBioMedicine 41 (2019) 244–255.
[29] Y. Zhang, J. An, Y. Shao, N. Yu, S. Yue, H. Sun, J. Zhang, W. Gu, Y. Xia, J. Zhang, Y. Xu, Z. Zhong, CD38-directed vincristine nanotherapy for acute lymphoblastic leukemia, Biomacromolecules 23 (2022) 377–387.
[30] J. Du, S. Yue, C. Li, J. Li, S. Zhao, Y. Dong, Y. Zhang, R. Cheng, H. Sun, Z. Zhong, Exogenous CD38 upregulation enables high-efficacy dually cascade targeted molecular therapy of leukemia, Nano Today 50 (2023) 101872.
[31] Y. Xia, J. An, J. Li, W. Gu, Y. Zhang, S. Zhao, C. Zhao, Y. Xu, B. Li, Z. Zhong, F. Meng, Transferrin-guided intelligent nanovesicles augment the targetability and potency of clinical PLK1 inhibitor to acute myeloid leukemia, Bioact. Mater. 21 (2023) 499–510.
[32] W. Zhu, H. Yu, M. Jia, C. Lin, Z. Yuan, X. Tan, P. Yan, Multi-targeting liposomal codelivery of cisplatin and rapamycin inhibits pancreatic cancer growth and metastasis through stromal modulation, Int. J. Pharm. 644 (2023) 123316.
[33] X. Zeng, Y. Zhang, X. Xu, Z. Chen, L. Ma, Y. Wang, X. Guo, J. Li, X. Wang, Construction of pH-sensitive targeted micelle system co-delivery with curcumin and dasatinib and evaluation of anti-liver cancer, Drug Deliv. 29 (2022) 792–806.
[34] Z. Zhang, H. Zhu, K. Xie, J. Lu, X. Chen, H. Wang, A self-assembling cytotoxic nanotherapeutic strategy for high drug loading and synergistic delivery of molecularly targeted therapies, Acta Biomater. 191 (2025) 398–411.
[35] M.W. Chao, M.J. Lai, J.P. Liou, Y.L. Chang, J.C. Wang, S.L. Pan, C.M. Teng, The synergic effect of vincristine and vorinostat in leukemia *in vitro* and *in vivo*, J. Hematol. Oncol. 8 (2015) 82.
[36] P. Dhyani, C. Quispe, E. Sharma, A. Bahukhandi, P. Sati, D.C. Attri, A. Szopa, J. Sharifi-Rad, A.O. Docea, I. Mardare, D. Calina, W.C. Cho, Anticancer potential of alkaloids: a key emphasis to colchicine, vinblastine, vincristine, vindesine, vinorelbine and vincamine, Cancer Cell Int 22 (2022) 206.
[37] S. Yue, J. An, Y. Zhang, J. Li, C. Zhao, J. Liu, L. Liang, H. Sun, Y. Xu, Z. Zhong, Exogenous antigen upregulation empowers antibody targeted nanochemotherapy of leukemia, Adv. Mater. 35 (2023) 2209984.
[38] S.F. Lin, C.N. Yeh, Y.T. Huang, T.C. Chou, R.J. Wong, Therapeutic inhibition of polo-like kinases in anaplastic thyroid cancer, Cancer Sci. 112 (2021) 803–814.
[39] Z. Yu, P. Deng, Y. Chen, S. Liu, J. Chen, Z. Yang, J. Chen, X. Fan, P. Wang, Z. Cai, Y. Wang, P. Hu, D. Lin, R. Xiao, Y. Zou, Y. Huang, Q. Yu, P. Lan, J. Tan, X. Wu, Inhibition of the PLK1-coupled cell cycle machinery overcomes resistance to oxaliplatin in colorectal cancer, Adv. Sci. 8 (2021) e2100759.
[40] J. Yang, P. Zhang, Y. Mao, R. Chen, R. Cheng, J. Li, H. Sun, C. Deng, Z. Zhong, CXCR4-mediated codelivery of FLT3 and BCL-2 inhibitors for enhanced targeted combination therapy of FLT3-itd acute myeloid leukemia, Biomacromolecules 25 (2024) 4569–4580.
[41] P. Tardi, S. Johnstone, N. Harasym, S. Xie, T. Harasym, N. Zisman, P. Harvie, D. Bermudes, L. Mayer, *In vivo* maintenance of synergistic cytarabine: daunorubicin ratios greatly enhances therapeutic efficacy, Leuk. Res. 33 (2009) 129–139.
[42] S. Buonamici, T. Trimarchi, M.G. Ruocco, L. Reavie, S. Cathelin, B.G. Mar, A. Klinakis, Y. Lukyanov, J.-C. Tseng, F. Sen, E. Gehrie, M. Li, E. Newcomb, J. Zavadil, D. Meruelo, M. Lipp, S. Ibrahim, A. Efstratiadis, D. Zagzag, J. S. Bromberg, M.L. Dustin, I. Aifantis, CCR7 signalling as an essential regulator of CNS infiltration in T-cell leukaemia, Nature 459 (2009) 1000–1004.
[43] F. Yang, W. Feng, H. Wang, L. Wang, X. Liu, R. Wang, C. Chen, X. Yang, D. Zhang, Q. Ren, G. Zheng, Monocyte-derived leukemia-associated macrophages facilitate extramedullary distribution of T-cell acute lymphoblastic leukemia cells, Cancer Res. 80 (2020) 3677–3691.
[44] Y. Dong, F. You, Y. Zhang, H. Sun, R. Cheng, S. Zhao, L. Yang, Z. Zhong, CD7 nanobody-based immuno-nanotoxin for targeted treatment of t-cell acute lymphoblastic leukemia, ACS Appl. Nano Mater. 7 (2024) 7195–7202.
[45] D. Chen, F.T. You, S.F. Xiang, Y.Y. Wang, Y.F. Li, H.M. Meng, G.L. An, T.T. Zhang, Z.X. Li, L.C. Jiang, H. Wu, B.J. Sheng, B.Z. Zhang, L. Yang, Chimeric antigen receptor T cells derived from CD7 nanobody exhibit robust antitumor potential against CD7-positive malignancies, Am. J. Cancer Res. 11 (2021) 5263–5281.
[46] R.M. Bertoli, P.D. Aplan, Y.J. Chung, Mechanism for bone marrow failure differs between acute myeloid and lymphoid leukemia, Cancer Res. 83 (2023) 3664.
[47] A.F. Al-Mashdali, M.A. Yassin, Osteolytic bone lesions as an initial presenting manifestation of acute lymphoblastic leukemia in adults, Blood 140 (2022) 11603–11604.
[48] S. Agarwal, J.D.S. Hanauer, A.M. Frank, V. Riechert, F.B. Thalheimer, C. J. Buchholz, *In vivo* generation of CAR t cells selectively in human CD4+ lymphocytes, Mol. Ther. 28 (2020) 1783–1794.
[49] Y. Shi, I.S. Kotchetkov, A. Dobrin, S.A. Hanina, V.K. Rajasekhar, J.H. Healey, M. Sadelain, GLUT1 overexpression enhances CAR T cell metabolic fitness and anti-tumor efficacy, Mol. Ther. 32 (2024) 2393–2405.